A preliminary assessment of low pressure, amphibolite-facies metamorphism in the upper Hyland River area (NTS 105H), southeast Yukon

David P. Moynihan[1]
Yukon Geological Survey, Whitehorse, YT

Moynihan, D.P., 2013. A preliminary assessment of low pressure, amphibolite-facies metamorphism in the upper Hyland River area (NTS 105H), southeast Yukon. *In:* Yukon Exploration and Geology 2012, K.E. MacFarlane, M.G. Nordling, and P.J. Sack (eds.), Yukon Geological Survey, p. 99-114.

ABSTRACT

The regional metamorphic grade in southeast Yukon is low, but amphibolite-facies metamorphism has affected regions adjacent to numerous mid-Cretaceous intrusions. In the upper Hyland River area, contact aureoles approximately 300 m wide are developed around the Hyland and Boundary plutons, which are members of the 97-94 Ma Tungsten plutonic suite. Andalusite + cordierite + biotite-bearing assemblages in the aureole of the Hyland pluton imply emplacement at ~2.5-3 kbar, equivalent to a depth of 9 to 11 km. Cordierite + biotite assemblages in the aureole of the adjacent Boundary pluton suggest emplacement at shallower levels (<~2.5 kbar or <9 km). Metamorphism associated with these intrusions took place after most regional deformation. In contrast, rocks adjacent to the older (*ca.* 106 Ma) Mount Billings batholith were metamorphosed syn-kinematically. Staurolite ± andalusite ± sillimanite-bearing assemblages in metapelites east of the Mount Billings batholith indicate metamorphism at deeper levels (~4 kbar, or 15 km depth), coincident with the formation of structures oblique to the regional trend.

[1]*david.moynihan@gov.yk.ca*

INTRODUCTION

In the upper Hyland River area of southeast Yukon (Fig. 1), deformed Neoproterozoic-Mississippian rocks of the Selwyn basin host numerous mid-Cretaceous intrusions of the Hyland and Tungsten plutonic suites (Roots *et al.*, 1966; Hart *et al.*, 2004; Hart and Lewis, 2006). The Hyland suite (106-96 Ma) is represented by large, heterolithic bodies that crop out southwest of the Hyland River, such as the Logan and Mount Billings batholiths (Fig. 1). These intrusions have tabular forms and contacts that are concordant with fabrics in the host rock (Hart and Lewis, 2006). Intrusions belonging to this suite are variably porphyritic, peraluminous or weakly peraluminous, biotite granite and granodiorite; muscovite-bearing phases are also locally present. Hyland suite rocks are weakly oxidized, with moderate magnetic susceptibilities and are associated with W ± Mo, Cu skarns, and distal Ag-Pb-Zn vein mineralization (Hart *et al.*, 2004).

The 97-94 Ma Tungsten suite (Gordey and Anderson, 1993; Hart *et al.*, 2004; Heffernan, 2004; Rasmussen *et al.*, 2006) is represented by small to moderate sized, discordant, biotite granite, monzogranite, and quartz monzonite intrusions. These bodies, which are restricted to the area northeast of the Little Hyland River (Fig. 1), are weakly to moderately peraluminous, ilmenite-bearing, and associated with significant W ± Mo, Cu skarn mineralization (*e.g.*, Cantung; Blusson, 1968).

The metamorphic grade in the Hyland River valley area is low (subgreenschist to lower greenschist-facies; chlorite zone), with the exception of areas directly adjacent to intrusions (Read *et al.*, 1991). Narrow, amphibolite-facies contact metamorphic aureoles surround intrusions of the Tungsten suite (Gordey and Anderson, 1993), whereas there is a large region of schist and gneiss of uncertain origin adjacent to the Mount Billings and Logan batholiths (Roots *et al.*, 1966; McLeod, 1982). In this paper, a preliminary assessment of each of these styles of metamorphism is presented, based on detailed fieldwork in two small areas. Area 1 (Fig. 1) includes part of the contact aureoles of two small, Tungsten suite intrusions. Area 2 (Fig. 1) lies within a region of schist and gneiss to the east of the Mount Billings batholith.

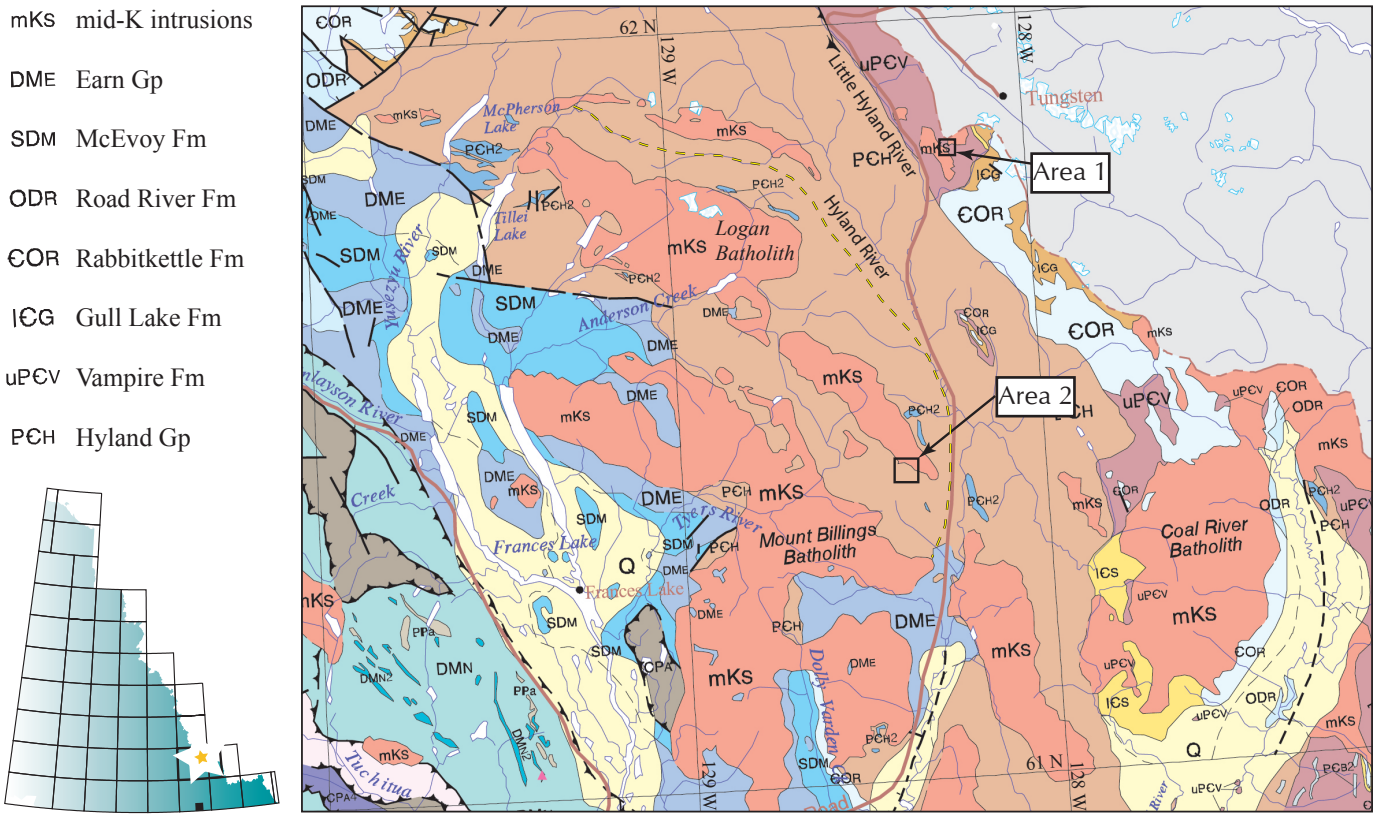

Figure 1. *Geology of the Upper Hyland River area, from Gordey and Makepeace (2003). The locations of the two study areas are marked with black boxes. The dashed yellow line marks the eastern boundary of the schist/gneiss belt adjacent to the Mount Billings and Logan batholiths (Roots et al., 1966).*

Estimates of pressure and temperature conditions during metamorphism are made based on mineral assemblages in metapelites. These assemblages are sensitive discriminants of pressure-temperature conditions and also record timing relationships between metamorphism and deformation.

As contact metamorphism adjacent to simple intrusions is fast in geological terms, pressure-sensitive mineral assemblages in aureoles provide a proxy for their depth of emplacement. In the case of contact aureoles surrounding the two small Tungsten suite intrusions that were studied (Area 1), pressure estimates are valid indicators of emplacement depth. Pressure estimates from rocks east of the Mount Billings batholith (Area 2) cannot be interpreted as providing a direct indication of its emplacement depth, as the timing relationships between metamorphism and plutonism in this area are unclear.

METHODS FOR ESTIMATING P-T CONDITIONS

Pressure-temperature estimates are made by comparing observed mineral assemblages (Table 1) with phase diagrams (equilibrium assemblage diagrams) that show thermodynamically predicted mineral assemblages as a function of pressure and temperature for the bulk composition of interest. For this study, phase diagrams were constructed in the model system K_2O-FeO-MgO-Al_2O_3-SiO_2-H_2O (KFMASH) using THERIAK/DOMINO software (de Capitani and Brown, 1987; de Capitani and Petrakakis, 2010) in conjunction with the thermodynamic database and solution models outlined in Spear and Pyle (2010). The KFMASH system accounts for the major index minerals that record variations in metamorphic grade. Garnet stability is not satisfactorily modelled in KFMASH; however, garnet is absent or a minor phase in the rocks under consideration and is not used for P-T estimates. The bulk composition of representative, homogeneous hand samples was determined by fusion XRF (major elements) and infrared spectroscopy (S, C) at Activation Laboratories Ltd. (Table 2). Samples were milled with mild steel. KFMASH compositions were derived from full compositions by projecting from ilmenite, pyrrhotite, albite and anorthite end-members of plagioclase, and by dropping MnO and P_2O_5. All mineral abbreviations used are from Kretz (1983).

HYLAND AND BOUNDARY PLUTON CONTACT AUREOLES

The Hyland and Boundary plutons are biotite quartz monzonite intrusions located on the east side of the Little Hyland River (Fig. 1; Blusson, 1968). The Hyland pluton (also known as the Tuna stock) lies entirely within Yukon, and the Boundary pluton overlaps the Yukon-NWT border. The two plutons are separated by a narrow septum of low grade country rock, around which this study area is centred (Fig. 2).

The Hyland and Boundary plutons are hosted by the Latest Proterozoic-Early Cambrian Vampire Formation. The Vampire Formation in this region is dominated by uniform, rusty brown weathering and steel grey to dark grey phyllite. Phyllite is locally interbedded with quartzite layers that are generally 1-3 cm thick, but are locally up to 30 cm (Fig. 2b).

The dominant foliation in the area (S_n) strikes NW/SE, parallel to the orogenic trend (Fig. 3). It generally dips NE at 40-70° in the southwest part of the area and dips steeply towards the SW or NE in the northeast part of the area. S_n is locally overprinted by kink bands that have steeply-dipping axial planes and approximately down-dip axes (F_{n+1}). These kink bands post-date development of the contact aureoles and are best developed in low-grade phyllites, which retain a well-defined cleavage.

The pluton-Vampire Fm contact is offset by a number of steeply-dipping, SW-trending normal faults with downthrow to the NW (Fig. 3). These faults are sub-parallel to axial planes of the kink bands, and also have the same orientation as 1) a number of fine-grained, biotite and amphibole-bearing mafic dikes, and 2) an array of quartz-tourmaline veins that transect the Boundary aureole.

HYLAND PLUTON CONTACT AUREOLE

The Hyland pluton, which was emplaced at 97.1 ± 2.0 Ma (U-Pb monazite; Heffernan, 2004), is elongate in a NW direction and underlies an area of approximately 9×2.5 km. The roof of the pluton is preserved around the topographically highest point near the centre of the intrusion. The southwest boundary of the pluton dips steeply, whereas its northeast and southeast boundaries have gentle to moderately steep outward dips. Along the part of the northeast margin that was studied, the pluton-country rock contact dips NE, at an angle of approximately 30-50°, and is locally concordant with the dominant cleavage in the country rock (Fig. 3). The pluton is a biotite quartz monzonite (Streckheisen, 1973); it includes a megacrystic internal phase and an equigranular outer phase. The pluton is undeformed, except around its margin, where a NW-trending foliation and shallowly-plunging lineation is variably developed (Fig. 2c).

Table 1. *Sample locations and mineral assemblages for all samples from which thin-sections were examined.* P *indicates that minerals are pseudomorphed.*

Sample #	UTM E	UTM N	Elev (m)	Grt	Sil	St	And	Crd	Bt	Chl	Ms	Qtz
Area 1												
12-DMO-190	541125	6856906	1442				P	P	X	X	X	X
12-DMO-191	540875	6856771	1512				P	P	X		X	X
12-DMO-192	540710	6856650	1553				X	P	X		X	X
12-DMO-193	540579	6856584	1578				X	P	X		X	X
12-DMO-196	541055	6856405	1461				P	P	X		X	X
12-DMO-197	541283	6857046	1441				P		X	X	X	X
12-DMO-198	541221	6857214	1445							X	X	X
12-DMO-199	541498	6857272	1490							X	X	X
12-DMO-201	542160	6857210	1700							X	X	X
12-DMO-202	542246	6857259	1717					P	X	X	X	X
12-DMO-203	542386	6857284	1707					P	X		X	X
12-DMO-204	542551	6857204	1692					P	X		X	X
12-DMO-205	542510	6857459	1691				X	P	X		X	X
12-DMO-206	542380	6857703	1630				X	P	X		X	X
12-DMO-207	542318	6857732	1584					P	X		X	X
12-DMO-211	541927	6857335	1657							X	X	X
12-DMO-212	541934	6857368	1649					P	X	X	X	X
12-DMO-213	541951	6857403	1651					P	X	X	X	X
12-DMO-216	541772	6858023	1659					P	X		X	X
12-DMO-218	541276	6858182	1750							X	X	X
12-DMO-219	541340	6857925	1724							X	X	X
12-DMO-220	541495	6857879	1675					P	X	X	X	X
12-DMO-222	541686	6857521	1562							X	X	X
12-DMO-224	541737	6856300	1339				P	P	X		X	X
12-DMO-225	541578	6856497	1410				X	X	X		X	X
Area 2												
12-DMO-227A	530954	6810222	1585	X	X	X	X		X			X
12-DMO-227B	530954	6810222	1585		X	X	X		X			X
12-DMO-228A	530758	6810013	1633	X		X			X			X
12-DMO-228B	530758	6810013	1633	X	X	X			X		X	X
12-DMO-229	530766	6809718	1969	X	X	X	X		X		X	X
12-DMO-230	530757	6809486	1966		X	X			X		X	X
12-DMO-231	531024	6809250	1909	X	X	X			X		X	X
12-DMO-232	531285	6809047	1877	X	X	X			X		X	X
12-DMO-234A	531491	6808800	1922		X	X	X		X			X
12-DMO-234B	531491	6808800	1922		X	X	X		X			X
12-DMO-234C	531491	6808800	1922		X	X	X		X		X	X
12-DMO-235	531905	6808626	1936			X	X		X		X	X
12-DMO-236	532298	6808638	1968		X	X	X		X	X	X	X
12-DMO-237	532626	6808641	2015	X		X	X		X			X
12-DMO-238	533099	6808398	2045			X	X		X			X
12-DMO-240	533506	6807835	1962			X	X		X		X	X
12-DMO-241	533398	6807609	1972			X	X		X	X	X	X
12-DMO-242	531600	6809253	1763		X	X	X		X			X

Table 2. *Whole rock compositions from XRF (major elements) and infrared spectroscopy (S, C).*

Sample #	SiO2 %	Al2O3 %	Fe2O3(T) %	MnO %	MgO %	CaO %	Na2O %	K2O %	TiO2 %	P2O5 %	LOI %	Total %	C %	S %	Mg#
12-DMO-190	58.15	21.86	7.29	0.05	1.32	0.22	0.58	4.16	0.96	0.12	3.81	98.56	0.03	0.01	0.29
12-DMO-192	53.65	24.55	8.70	0.18	1.85	0.17	1.08	3.69	0.95	0.13	4.29	99.29	0.02	0.01	0.32
12-DMO-203	59.36	20.22	8.84	0.07	1.97	0.12	0.60	3.43	1.00	0.12	4.00	99.77	< 0.01	< 0.01	0.33
12-DMO-205-2*	40.09	32.81	10.23	0.12	2.54	0.59	0.45	5.68	1.66	0.20	5.03	99.46	0.02	< 0.01	0.37
12-DMO-225-B*	42.00	34.12	7.44	0.09	1.74	0.08	0.54	6.96	1.32	0.06	4.15	98.55	0.03	0.04	0.36
12-DMO-229	49.57	25.34	9.94	0.09	2.26	0.55	2.08	4.41	1.13	0.14	2.98	98.53	0.04	0.12	0.34
12-DMO-231	56.00	22.47	9.14	0.07	2.16	0.40	1.11	3.80	1.08	0.11	2.51	98.89	0.04	0.10	0.35
12-DMO-234A	35.77	35.59	14.72	0.14	3.43	0.21	0.20	3.96	1.95	0.16	3.04	99.25	0.07	0.03	0.35
12-DMO-241	52.12	24.57	8.46	0.05	1.70	0.28	0.89	5.26	1.26	0.10	4.31	99.06	0.26	0.10	0.33
12-DMO-242	40.15	33.43	12.54	0.11	2.91	0.54	1.29	4.28	1.57	0.11	2.35	99.34	0.04	0.07	0.35

Mg# = Mg/(Mg+Fe) in KFMASH
***adjacent to veins, not typical metapelite**

In the low grade area, outside of the contact aureole, metapelite is phyllitic and comprises fine-grained muscovite, chlorite, quartz, ilmenite, and other minor phases. Aligned muscovite and chlorite define a penetrative cleavage; chlorite also forms rounded, slightly elongate porphyroblasts approximately 0.1 mm long (Fig. 4a). The contact aureole includes a phyllitic outer part and a yellow-weathering, hornfelsic inner part. The outer margin of the aureole is marked by the first appearance of small, sparsely distributed spots in the grey phyllite (Fig. 2d). These spots are small porphyroblasts of andalusite and cordierite, whose presence also coincides with the first appearance of tiny biotite crystals (Fig. 4b). Apart from these spots, the rock is similar to phyllites outside the contact aureole, with a well-developed cleavage and phyllitic sheen. With increasing proximity to the pluton, the proportion of chlorite decreases to zero and cordierite, andalusite, and biotite crystals become larger and more abundant (Fig. 4c). Well-preserved cordierite was only observed in a single sample; elsewhere it is pseudomorphed by a fine-grained aggregate rich in chlorite and muscovite. Andalusite is generally partly replaced by muscovite and pokiloblastic, but locally forms well-preserved, idoblastic, inclusion-poor crystals (Fig. 4d). Chlorite-free rocks in the inner parts of the aureole are yellow-brown weathering hornfels with knobbly surfaces due to differential weathering of abundant porphyroblasts (Fig. 2e).

In the outer part of the Crd + And (Chl-free) zone, S_n is discernible but is largely annealed (it does not form a prominent plane of weakness in the rock). In this region, porphyroblasts are superimposed on the matrix foliation (S_n), and there is limited evidence for post-porphyroblast strain in the form of minor deflection of the foliation around porphyroblasts. In most of the Crd + And zone, however, deformation accompanied or post-dated contact metamorphism; cordierite and andalusite porphyroblasts host strain shadows (Fig. 4d), biotite crystals help define the matrix fabric, and curved inclusion trails in andalusite are commonly oblique to, and discontinuous with, the matrix foliation. In well-foliated rocks, micas and deformed pseudomorphs after cordierite define a gently-plunging lineation, approximately parallel to that in the marginal phase of the pluton.

The distance of the And + Crd-in isograd to the pluton contact is approximately 660 m (Fig. 3); however, as the pluton contact dips northeast under this zone, the true thickness is ~270 m (assuming a 40° dip).

The widespread development of Crd + Bt + Ms + Qtz assemblages in the Hyland aureole adjacent to biotite-free, chlorite-bearing phyllites suggests the Crd + And isograd reflects a full-system metamorphic reaction equivalent to the univariant (in KFMASH) reaction:

$$Chl + Ms + Qtz = And + Crd + Bt + H_2O.$$

A single sample with the assemblage Chl + Bt + And + Ms + Qtz on the margin of the aureole suggests the divariant (in KFMASH) reaction:

$$Chl + Ms + Qtz = Bt + And + H_2O.$$

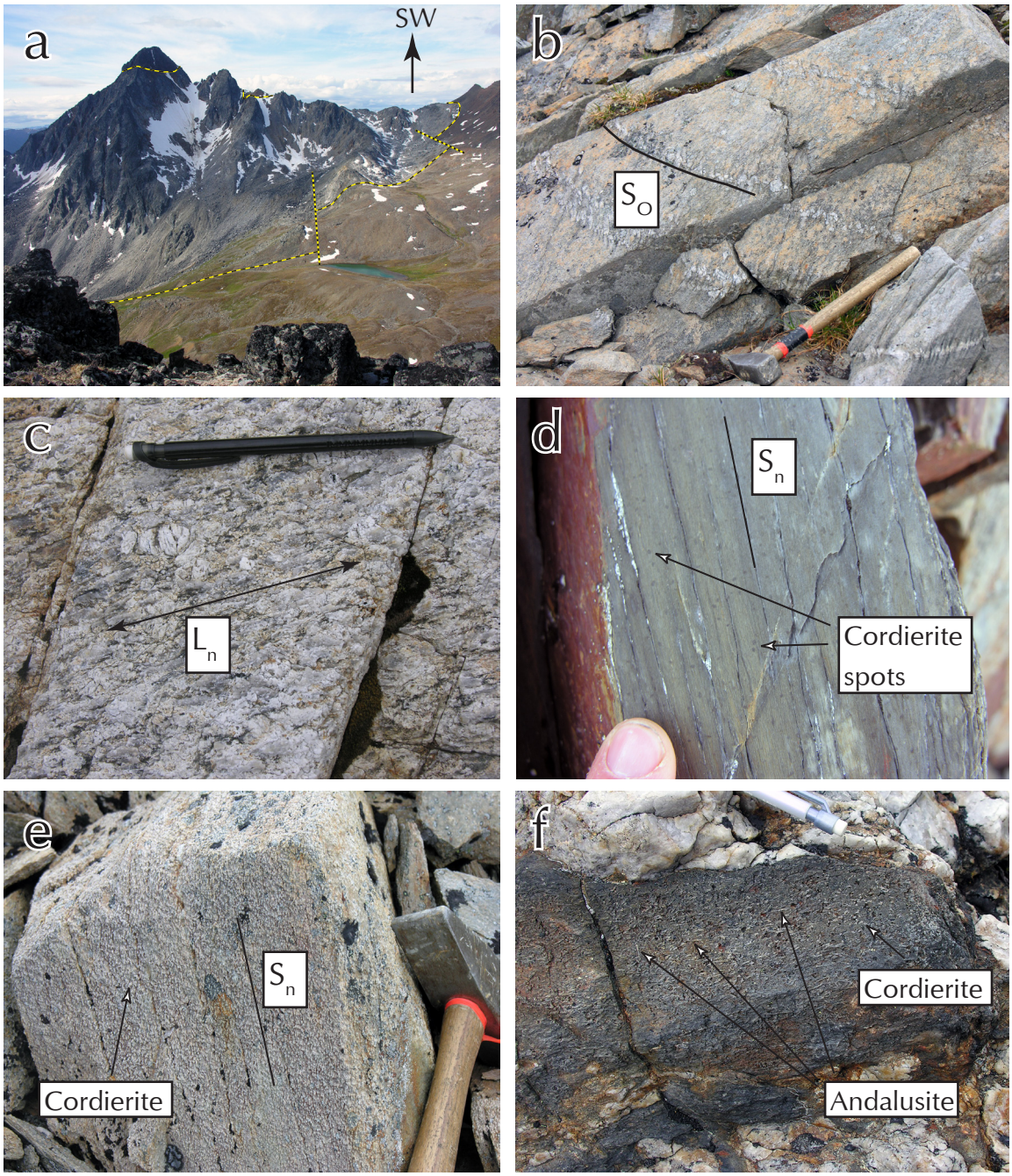

Figure 2. *a) View to the SW towards part of the NE margin of the Hyland pluton. The upper boundary of the pluton dips gently to the NE and is offset by SW-trending faults. Elevation difference between the lake and the peak is approximately 500 m. Pluton outline (long dash) and faults (short dash) are outlined by dashed yellow lines. b) Bedding (S_0) in metasedimentary rock of the Vampire Formation defined by thin, pale grey, fine-grained quartzite layers. The intervening rock is yellow-weathering metapelitic hornfels. Hammer for scale. c) Foliated and lineated, weakly porphyritic marginal phase of the Hyland pluton. The lineation plunges gently to the SE, approximately parallel to the long axis of the intrusion. Pencil for scale. d) Spotted phyllite from the outer part of the contact metamorphic aureole. The rock is a well-cleaved grey phyllite containing scattered small (<1 mm), ovoid cordierite porphyroblasts. Finger for scale. e) Metapelitic hornfels from the inner part of the Boundary pluton aureole. The rock contains abundant mm-scale cordierite porphyroblasts. Foliation is discernible, but the rock is more massive than in regions of lower metamorphic grade. Hammer for scale. f) Elongate andalusite porphyroblasts in metapelite adjacent to a deformed quartz vein. Cordierite is widely developed in the Boundary pluton aureole whereas andalusite is restricted to the margins of veins such as this one. Pencil for scale.*

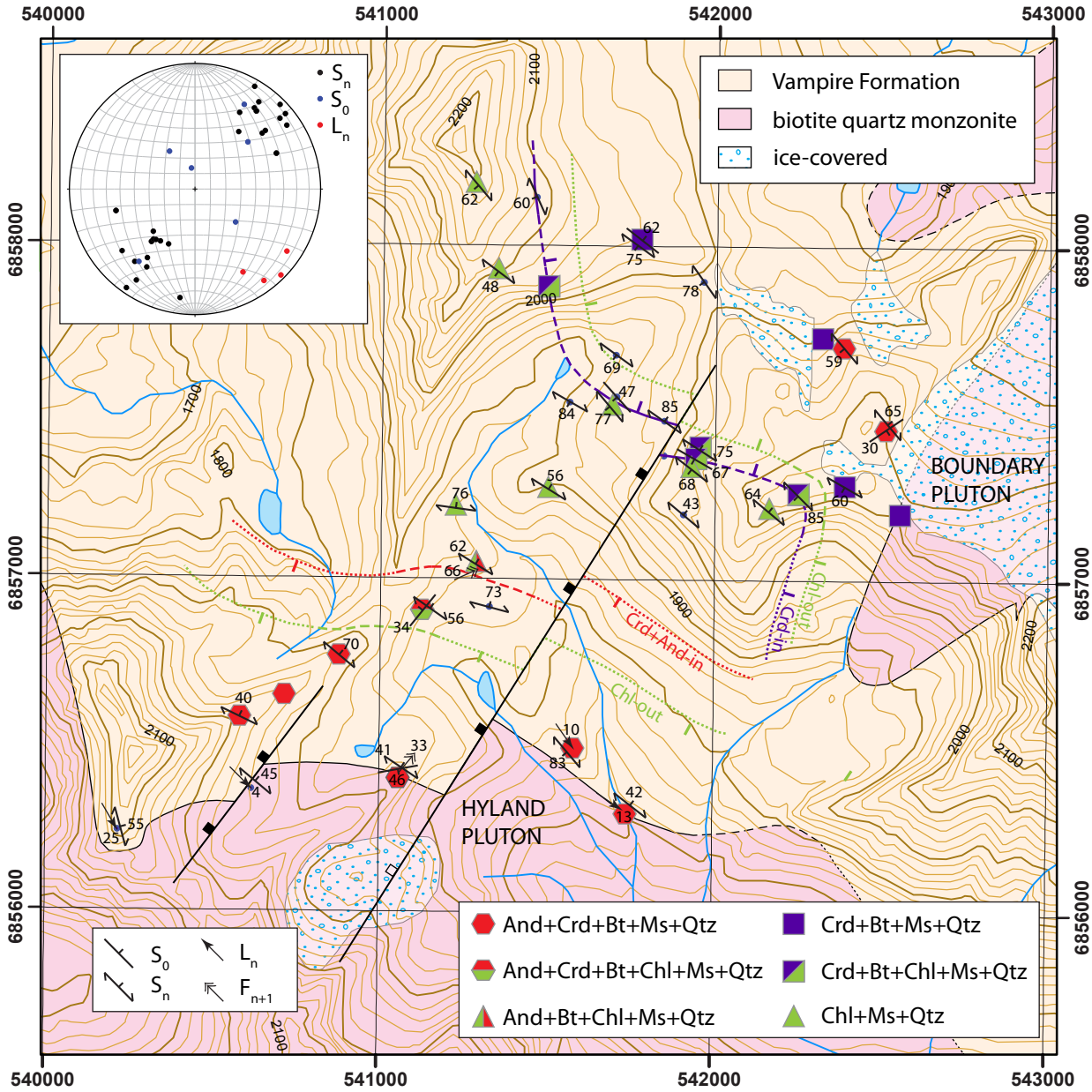

Figure 3. *Map of parts of the Hyland and Boundary plutons and their contact aureoles, showing mineral assemblages and isograds. Structural measurements are compiled on the equal area, lower hemisphere stereonet (inset). Grid lines spaced at 1 km intervals; UTM coordinates are NAD 83.*

BOUNDARY PLUTON CONTACT AUREOLE

The Boundary pluton underlies approximately 9 km^2 on either side of the Yukon-NWT border. It is an equant body with a protrusion on its SW side whose contacts trend SW and dip steeply. The Boundary pluton is an undeformed to weakly deformed biotite quartz monzonite (Streckheisen, 1973) that crosscuts foliation in the country rock (Fig. 8).

The textural changes developed in the Boundary aureole are similar to those described above for the Hyland contact aureole. Unlike the Hyland aureole, however, andalusite is not developed in typical metapelitic rocks. Instead, the assemblage Crd + Bt + Ms + Qtz is widespread, with chlorite also present in the outer parts of the aureole. The distance from the Crd-in isograd to the pluton boundary is approximately 300 m. As is the case in the Hyland aureole, cordierite has been replaced by a fine-grained aggregate rich in chlorite and muscovite.

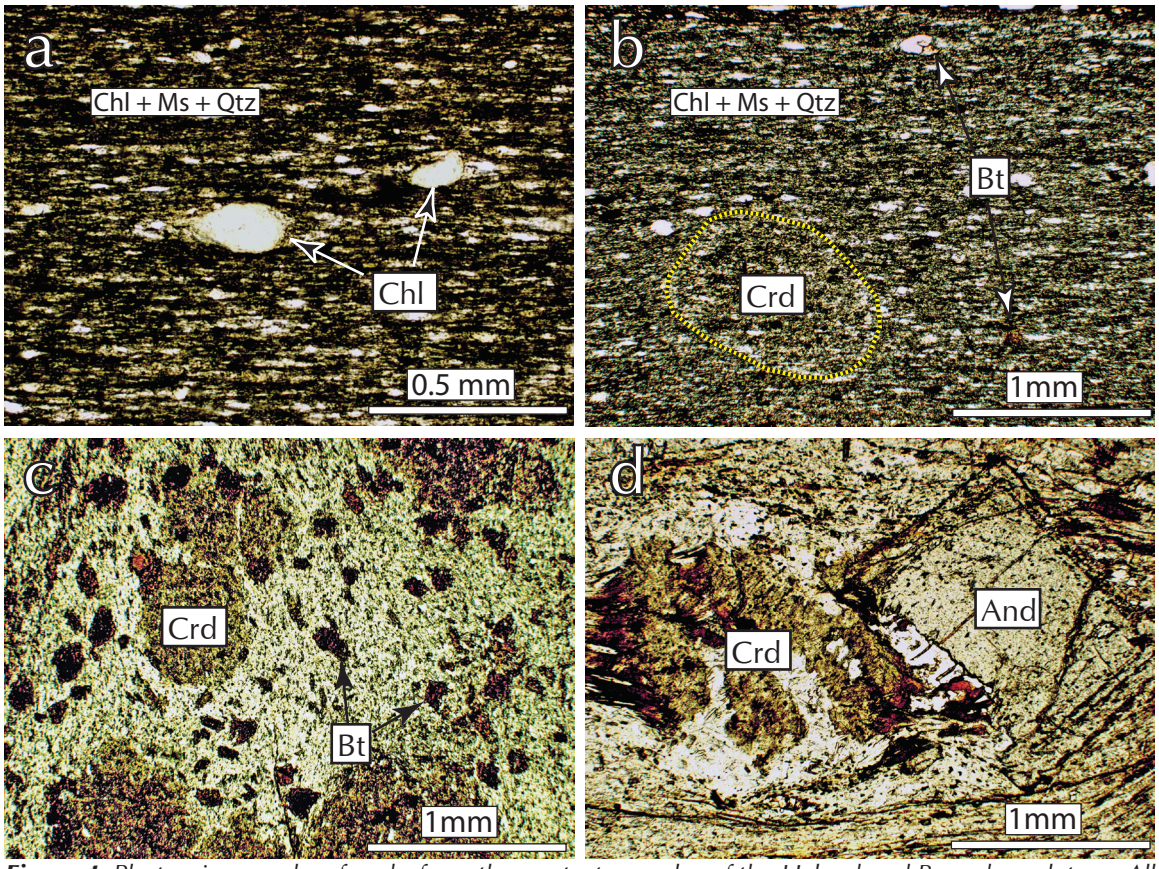

Figure 4. *Photomicrographs of rocks from the contact aureoles of the Hyland and Boundary plutons. All photomicrographs taken in plane polarized light (PPL). a) Phyllite from the low grade area between the Hyland and boundary aureoles. The well-foliated matrix is dominated by fine-grained chlorite, muscovite and quartz, with small rounded chlorite porphyroblasts. b) Spotted phyllite from the outermost part of the Boundary aureole (~at the Crd+Bt isograd). The rock contains sparse, inclusion-rich cordierite porphyroblasts and small biotite crystals. The matrix of the rock is otherwise similar to that outside the aureole, with abundant chlorite. c) Crd+Bt assemblage from the hornfelic inner part of the Boundary aureole. Crd and Bt crystals are larger and more abundant, and there is no primary chlorite. d) Idioblastic andalusite and pseudomorphed cordierite from the Hyland aureole. Syn-kinematic growth is suggested by some wrapping of the porphyroblasts by the matrix but also overgrowth of the matrix foliation (see top of the And crystal).*

There is less evidence for syn-post metamorphic deformation in the Boundary aureole compared with the Hyland aureole. The aureole includes some well-foliated, heavily veined zones but these are uncommon. In general, there is only slight deflection of S_n around cordierite porphyroblasts.

Although andalusite is absent from typical metapelite in the aureole, the assemblage And + Crd + Bt + Ms + Qtz was observed in two locations within the aureole. In each case, andalusite is restricted to a zone of dark grey rock on the margin of deformed quartz veins (Fig. 2f). This rock, which is anomalously Al-rich and Si-poor (12DMO-205-2; Table 2) extends approximately 15 cm from the veins and grades outwards into typical metapelite with a Crd + Bt (And-free) assemblage.

The Crd-in isograd does not conform to the map outline of the Boundary pluton. Instead, an extensive region of Crd + Bt hornfels is developed in the area to the west of the pluton. This suggests that the Boundary pluton extends underneath this region, or that erosion has removed igneous rock from above the land surface.

In the Boundary aureole, the development of the metamorphic assemblage Crd + Bt from Chl + Ms-bearing phyllites suggests a reaction with the form:

$$Chl + Ms + Qtz = Crd + Bt + H_2O$$

(Divariant in KFMASH).

PRESSURE-TEMPERATURE CONDITIONS, HYLAND AND BOUNDARY AUREOLES

The assemblages Crd + Bt + Ms + Qtz and And + Crd + Bt + Ms + Qtz indicate metamorphism at intermediate temperatures and low pressure. The P-T stability range of each of these assemblages is illustrated using an equilibrium assemblage diagram, constructed using a mean composition representative of the Vampire Formation (Fig. 5a). For this composition, And + Crd + Bt + Ms + Qtz is predicted to form in the pressure range 2.5-3 kbar, whereas Crd + Bt + Ms + Qtz assemblages indicate P<~2.5 kbar.

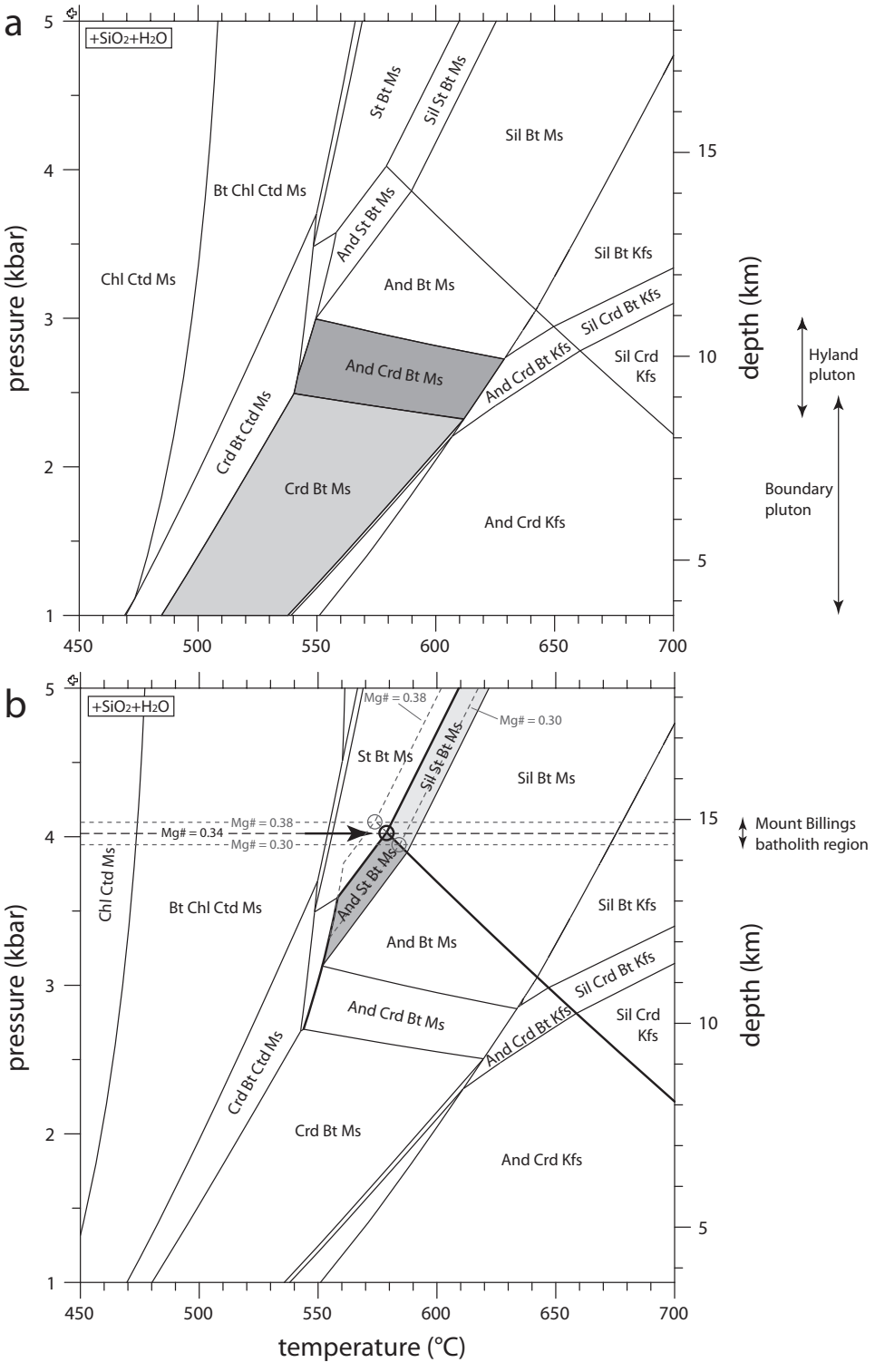

Figure 5. *a) Equilibrium assemblage diagram for the composition representing the mean of three Vampire Fm metapelite samples (Mg/(Mg+Fe)=0.32). b) Equilibrium assemblage diagram for the composition representing the mean of 3 muscovite-bearing Hyland Group metapelites (Mg/(Mg+Fe) = 0.34). The Al_2SiO_5-in and the And-Sil phase boundaries are marked with thick lines. In most rocks, andalusite grew directly from staurolite, but in some samples staurolite breakdown produced sillimanite. This suggests the pressure during metamorphism is approximated by the position of the intersection between the Al_2SiO_5-in and the And-Sil boundaries (~4 kbar, ~15 km depth). The position of the Al_2SiO_5-in boundary is also shown for two modified compositions with Mg/(Mg+Fe) of 0.30 and 0.38, respectively (dashed lines); these compositions were derived by varying the Fe:Mg ratio while keeping values for other elements unchanged. These Mg/(Mg+Fe) values were chosen arbitrarily to illustrate the effect of variation in bulk composition on the P-T position of the intersection between the Al_2SiO_5-in and And-Sil boundaries. See text for discussion.*

Whereas the Hyland aureole contains the assemblage And + Crd + Bt + Ms + Qtz, the Boundary aureole lacks andalusite. This difference can be explained by either a difference in pressure (depth of intrusion), or by a systematic difference in the bulk composition of the host rocks. For a fixed pressure, the andalusite-bearing assemblage is favoured by more Fe and Al-rich compositions. In this case, the close proximity of the isograds in the same phyllite suggests a difference in pressure is the most plausible explanation for the lack of andalusite in the metapelite of the Boundary pluton. A systematic difference in composition is unlikely, as the plutons were intruded across a folded rock sequence and even small, non-systematic differences would complicate a simple trend. The suggestion that the Boundary pluton was intruded at a slightly higher level than the Hyland pluton is compatible with the semi-concordant nature of the Hyland pluton and the higher degree of deformation recorded in the pluton and its aureole.

All of the samples from the Vampire Formation that were analysed by XRF are high-Al metapelites that plot above the garnet-chlorite tie line on an AFM diagram (Fig. 6). Chloritoid is predicted to be stable at low metamorphic grade for each of these measured bulk rock compositions (Fig. 5), but is not present in low-grade rocks between the two contact aureoles. This discrepancy may reflect inadequacies in the projection scheme (Fig. 6), and/or the thermodynamic data and solutions models used (Fig. 5); alternatively, it may indicate relative enrichment in Al due to mass transfer during metamorphism (Ague, 1991). Another possibility, that the low-grade rocks had significantly different primary compositions compared with those within the aureoles, is unlikely.

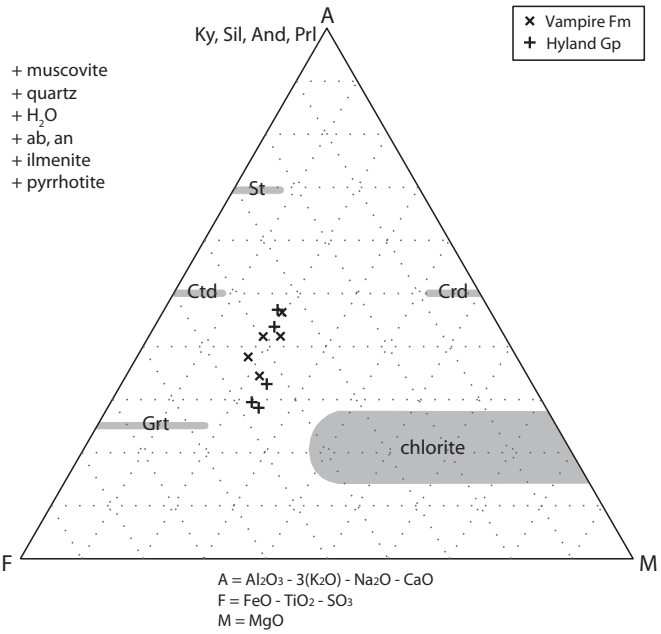

Figure 6. *AFM diagram showing all analysed samples. Mg/(Mg+Fe) in typical metapelite ranges from 0.29-0.34. Samples are projected from end-member muscovite, quartz, H_2O, albite, anorthite, ilmenite, and pyrrhotite. Mineral fields from Spear (1993). Biotite plots below the diagram as it has negative A values.*

METAMORPHISM OF THE HYLAND GROUP EAST OF THE MOUNT BILLINGS BATHOLITH

The second area studied in detail is located northeast of the Mount Billings batholith (Area 2; Fig. 1). This area lies within an extensive region of schist and gneiss that mantles the Logan batholith and the eastern side of the Mount Billings batholith (Roots *et al.*, 1966). Structures in this schist-gneiss belt are discordant with the regional trend and many intrusions have complex border zones up to 400 m wide which contain a mixture of migmatite and inclusions of country rock (*ibid*). Heffernan (2004) reported a U-Pb zircon crystallization age of 106.4 ± 0.4 Ma from the Mount Billings batholith and three U-Pb monazite crystallization ages from the Logan batholith in the range 101-106 Ma.

The country rock, which is assigned to the Hyland Group by Gordey and Makepeace (2003), comprises a monotonous sequence of pelitic and semipelitic schist (Fig. 7a). The schist is pale brownish-yellow with a rusty brown weathering colour. Foliation in the schist dips 20-40° to the southeast and a mineral lineation plunges southeast, approximately down the dip of the foliation. The mineral lineation is defined by mica, and most conspicuously, sillimanite. Locally, crenulations with the same orientation as the mineral lineation are also developed. Compositional layering is generally parallel to the foliation, and high strain is indicated by the presence of rootless isoclinal folds with axial planes parallel to the foliation. These fabrics are crosscut by a weakly deformed biotite granodiorite intrusion of presumed mid-Cretaceous age (northeast corner of Figure 8) and similar smaller bodies. They are also cut by dikes of unfoliated quartz-feldspar porphyry (Fig. 7d) and fine-grained, amphibolite bearing mafic dikes.

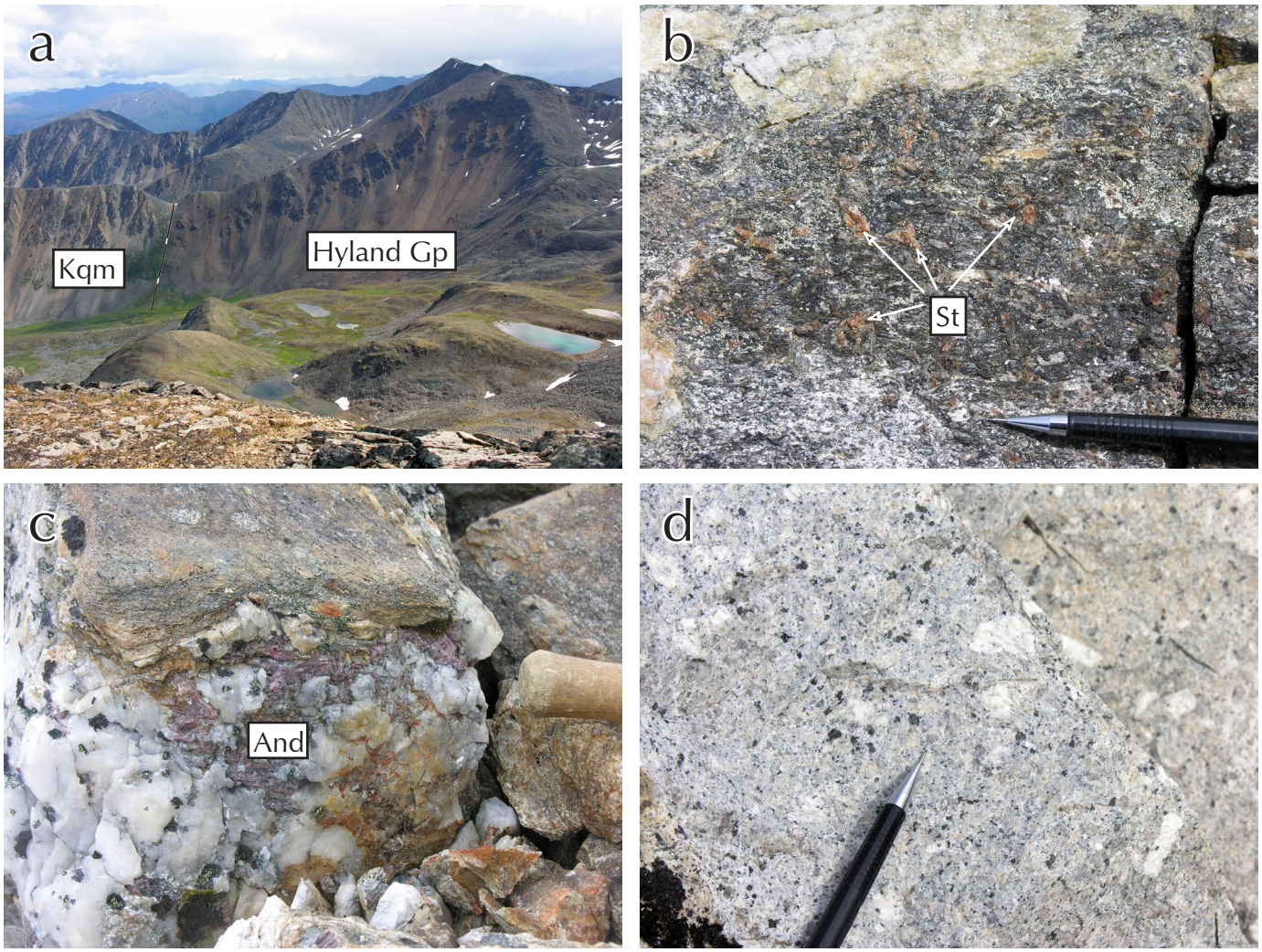

Figure 7. *a) View south towards the contact between rusty brown metapelite of the Hyland Group and a quartz monzonite intrusion of presumed mid-Cretaceous age. The foliation/lineation in the Hyland Group is truncated by the intrusion. Elevation difference between the valley bottom and the peak on the right hand side is approximately 200 m. b) Prominent honey-brown staurolite porphyroblasts in metapelitic schist. Metapelitic rocks in the area also typically contain andalusite, biotite, quartz, plagioclase ± sillimanite ± muscovite ± garnet. Pencil for scale. c) Vein composed of quartz and pink andalusite. Quartz-andalusite veins are common in the metapelitic schists and are deformed within the dominant foliation. Hammer handle for scale. d) Quartz-feldspar porphyry dike that crosscuts the foliation/lineation in metapelitic schists. Phenocrysts of euhedral to corroded quartz, plagioclase, K-feldspar and chloritized mafic phenocrysts sit in a fine-grained quartzofeldspathic matrix. Pencil for scale.*

Metapelitic schists in the area contain Qtz + Plag + Bt + Ilm + St + Al_2SiO_5(Sil and/or And) ± Ms ± Grt ± Sp (Table 1; Figs. 7b and 9). Staurolite forms porphyroblasts with irregular, embayed margins and is generally surrounded by a mantle of andalusite (Fig. 9b,d). In samples that lack andalusite but contain sillimanite (n=4), staurolite is rimmed by muscovite that is generally aligned parallel to S_n (Fig. 9c). Larger staurolite crystals are commonly twinned. Andalusite typically forms large blocky crystals, many with one or more staurolite inclusions. Andalusite is commonly pokiloblastic (Fig. 9d), and in some cases forms extensive, optically continuous, net-textured sheets parallel to compositional layering. Some crystals display pink segments, particularly in their cores (Fig. 9a). In two samples, green spinel is included within andalusite adjacent to embayed staurolite inclusions. Sillimanite occurs in the form of fibrolite in and/or around crystals of biotite (Fig. 9e). Garnet is present in small quantities in some rocks; crystals are generally small and have irregular, embayed margins (Fig. 9f).

The schistosity (S_n) is defined by preferentially aligned biotite and, where present, sillimanite and/or muscovite. Staurolite and andalusite contain inclusion trails, and andalusite crystals are wrapped by S_n. These observations indicate that deformation took place during the growth of staurolite, andalusite, and sillimanite.

Deformed quartz veins hosted by metapelitic schist commonly contain large, zoned crystals of pink andalusite (Fig. 7c). These veins locally crosscut the schistosity but are generally elongated parallel to the schistosity and wrapped by it; this suggests that the veining accompanied formation of S_n.

Metapelites throughout the study area contain andalusite; in contrast, sillimanite is restricted to its northwest part. The orientation of the sillimanite isograd is largely unconstrained due to the location of sampling sites (Fig. 8). Peak metamorphism is not related to the granodiorite body (of presumed mid-Cretaceous age) in the northeast part of the area because the syn-metamorphic schistosity is cut by this intrusion.

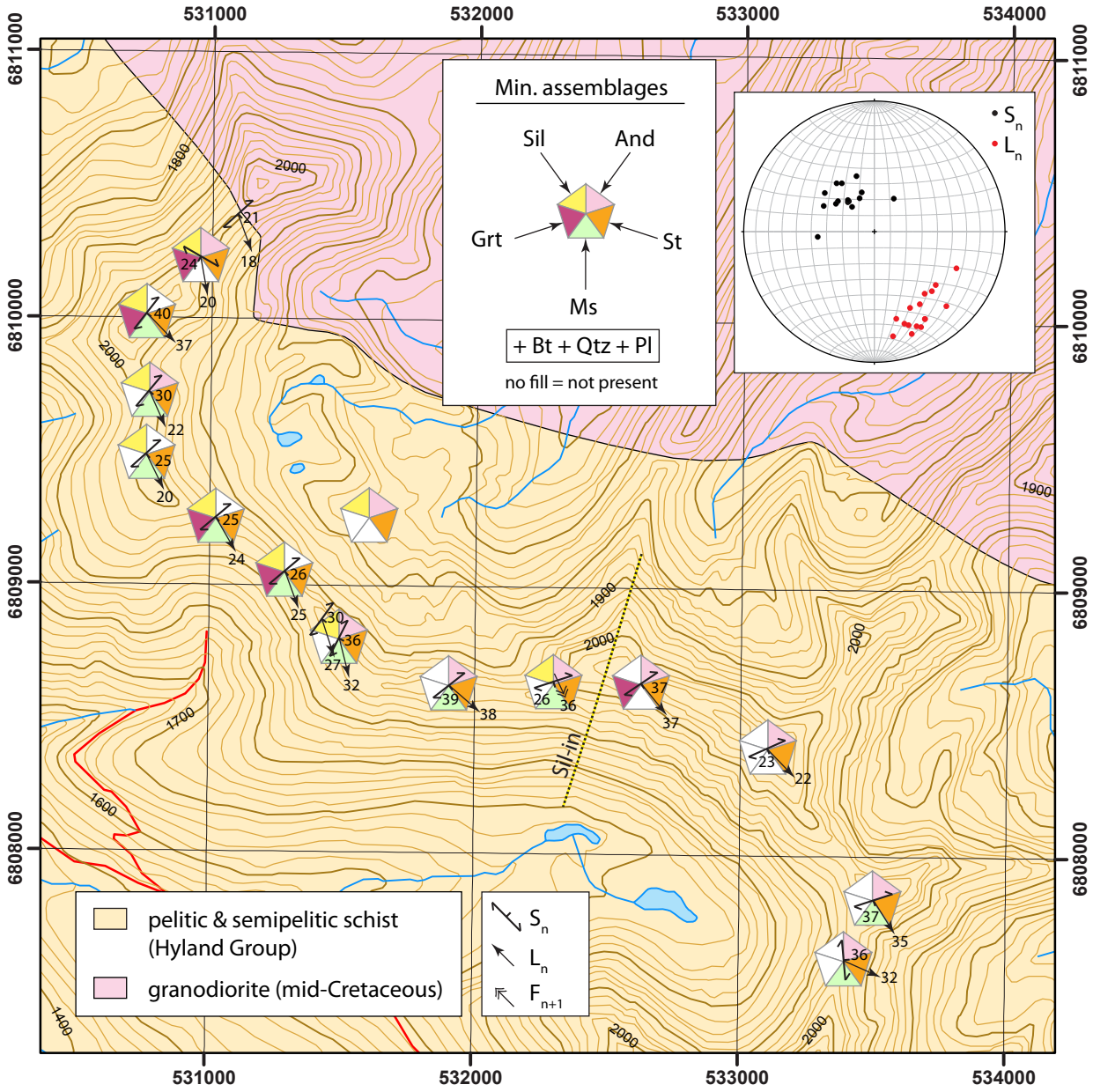

Figure 8. *Map of Area 2, east of the Mount Billings batholith showing mineral assemblages. Structural measurements are compiled on the equal area, lower hemisphere stereonet (inset). Grid lines spaced at 1 km intervals; UTM coordinates are NAD 83.*

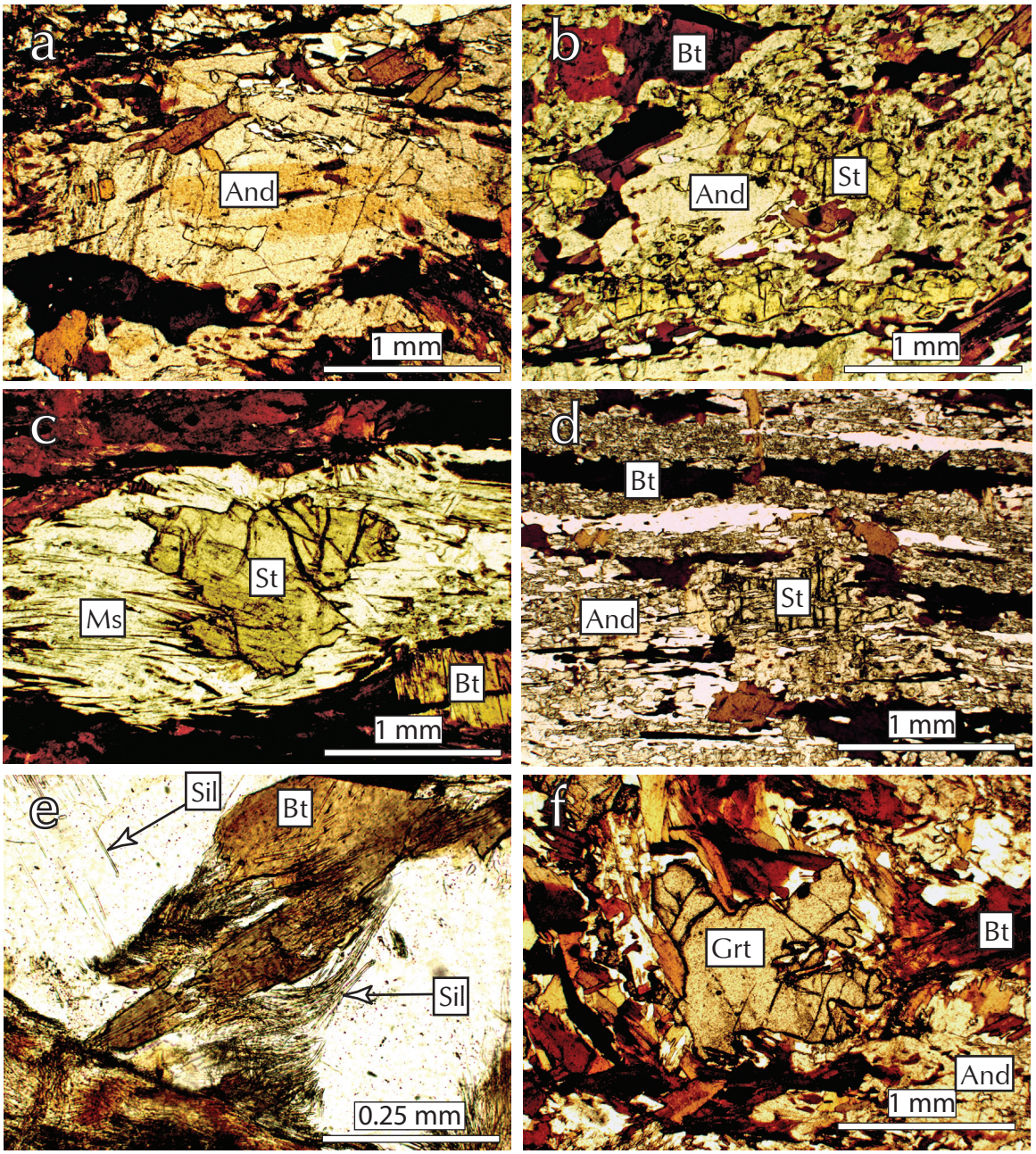

Figure 9. *Photomicrographs of metapelites from the area east of the Mt. Billings batholith, all taken in PPL. a) Andalusite displaying pink core and colourless rim. b) Embayed staurolite remnants surrounded by andalusite. c) Staurolite surrounded by a reaction rim of muscovite. d) Poikiloblastic andalusite with staurolite inclusion. e) Fibrolitic sillimanite on biotite and as inclusions in quartz. f) Embayed garnet crystal in metapelitic schist. Garnet is a minor constituent or is absent from schists in the area.*

REACTION HISTORY AND PRESSURE-TEMPERATURE CONDITIONS

Metapelites in Area 2 have low-variance assemblages and contain abundant non-equilibrium textures. Two Al_2SiO_5 polymorphs are present in most samples and staurolite is generally only preserved where mantled by andalusite, or locally muscovite.

The assemblage And + St + Bt + Ms, which occurs in the southeastern part of the area, is stable at intermediate temperatures (~550-575 °C) at a pressure of 3-4 kbar (Fig. 5b). Andalusite is predicted to grow at the expense of staurolite with increasing temperature in this field, and its high-T boundary marks the point at which staurolite is fully consumed. St + And (Sil-free) samples may have

reached their peak temperature in the And + St field, but the fact that staurolite occurs solely as inclusions in andalusite leaves open the possibility that staurolite was preserved above its predicted upper temperature limit as a result of its isolation from the remainder of the rock. In this case, the St + And field represents a lower bound on peak temperature conditions. The presence of sillimanite in otherwise similar samples from the northwest part of the area demonstrates further heating after St + And growth. The widespread preservation of andalusite in this area, in schists and quartz veins, suggests that the And-Sil boundary was not greatly overstepped. Significantly higher temperatures (T>625-650 °C) are ruled out by the widespread occurrence of the sub-assemblage Ms + Qtz (Fig. 5b).

In samples that contain sillimanite but lack andalusite, staurolite is surrounded by pseudomorphous aggregates of muscovite. This muscovite is aligned in the plane of S_n and there is no evidence that the muscovite is a late retrograde phase, or other evidence for retrogression in the rock (no replacement of minerals such as biotite or garnet). The muscovite pseudomorphs are interpreted to have formed during growth of sillimanite from staurolite breakdown, as described by Guidotti (1968). Rocks in the area thus contain evidence for independent growth of andalusite and sillimanite during staurolite breakdown.

Aluminosilicate growth from staurolite breakdown is accounted for by a whole rock equivalent of the divariant KFMASH metamorphic reaction:

$$St + Ms + Qtz = Al_2SiO_5 + Bt + H_2O$$

Garnet is also present in some samples and may be a product of a similar (univariant in KFMASH) reaction.

The Al_2SiO_5-producing reaction intersects the polymorphic transition:

$$And = Sil$$

at approximately 4 kbar (Fig. 5b). Above this pressure sillimanite is predicted to grow at the expense of staurolite whereas below this pressure andalusite is produced. This intersection is equivalent to the boundary between bathozones 2-3 of Carmichael (1978), and facies series 2B-3 of Pattison and Tracy (1991). The evidence for independent growth of andalusite and sillimanite from staurolite within the small area studied suggests that the pressure coincided with this intersection at or close to the peak metamorphic temperature (Fig. 5b). The spatial overlap of samples with different reaction histories can be accounted for by small variations in bulk composition (Fig. 5b). The intersection point between the Al_2SiO_5-producing reaction and the And-Sil boundary occurs at a slightly higher pressure in rocks with a relatively high bulk rock Mg/(Mg + Fe) (Fig. 5b). Growth of sillimanite directly from staurolite breakdown is therefore favoured by relatively Fe-rich bulk compositions, while andalusite growth is predicted in more Mg-rich rocks at the same pressure. Similarly, the intersection point occurs at a slightly higher pressure in Al-rich rocks.

DISCUSSION

The sensitivity of mineral assemblages in metapelites to small differences in pressure within the andalusite stability field facilitates recognition of otherwise indistinguishable contrasts in the depths of metamorphism. While the absolute depths implied by these mineral assemblages are subject to ongoing refinement to thermodynamic databases and activity models, the relative depths implied by the assemblages are well established (*cf.*, Pattison and Vogl, 2005).

The Hyland pluton was intruded late syn-kinematically at 97.1 Ma and, based on its And + Crd-bearing aureole assemblage, was emplaced at ~2.5-3 kbar, equivalent to a depth of ~9-11 km. The absence of andalusite from metapelite in the aureole of the Boundary pluton suggests it was intruded at <~9 km, though a meaningful lower depth limit is not provided by the And + Crd assemblage. The largely post-kinematic nature of the Boundary pluton, combined with the evidence in favour of a lower emplacement depth suggests that the Boundary pluton is slightly younger than the Hyland pluton; however, there is insufficient geochronological data to test this interpretation. A general point, applicable to metapelites here and elsewhere is that, whereas rocks with Crd + Bt-bearing aureoles may be prospective for shallow-level mineralizing processes, the presence of andalusite in metapelite typically indicates a greater depth of emplacement.

Staurolite ± andalusite ± sillimanite-bearing assemblages in the area to the east of the *ca.* 106 Ma Mount Billings batholith record metamorphism at ~4 kbar, equivalent to a depth of ~15 km. The spatial pattern, whereby amphibolite-facies rocks are restricted to the margins of the Mount Billings and Logan batholiths suggests low-pressure metamorphism in this area is related to plutonism, as does the reported presence of migmatite along batholith-country rock boundaries. This interpretation conflicts with that of Roots *et al.* (1966), who suggested

that syn-kinematic metamorphism was unrelated to Cretaceous plutonism and took place prior to deposition of the Devonian-Mississippian Earn Group, rocks belonging to which are "essentially non-schistose".

Mapping is required to establish the spatial and timing relationships among deformation, metamorphism, and plutonism in the area. While Roots *et al.* (1966) provided no indication that rocks of the Mt. Billings batholith are deformed, according to Archibald *et al.* (1982) they are at least locally foliated. The high strain that accompanied heating is not typical of contact metamorphism, but regional deformation, burial, and radiogenic heating alone generally cannot account for the elevated geothermal gradient required for low-pressure, amphibolite-facies metamorphism (England and Thompson, 1984). Whereas structures outside this belt follow the NW-NNW orogenic trend, structures in the schist/gneiss have more variable orientations (Roots *et al.*, 1966), and in the area studied, the foliation is orogen-perpendicular. The timing relationships between medium-grade fabrics and low grade structures outside this belt remain to be determined, as does the tectonic significance of the metamorphic and structural variation.

ACKNOWLEDGEMENTS

Thanks to Nikollet Kovacs for assistance in the field, and to Terralogic Ltd. who provided logistical support for the field work. Doug Tinkham (Laurentian University) translated the thermodynamic data base and solution models of Spear and Pyle (2010) into a form compatible with Theriak/Domino. Thanks to Lee Pigage for reviewing the manuscript and suggesting improvements.

REFERENCES

Ague, J.J., 1991. Evidence for major mass transfer and volume strain during regional metamorphism of pelites. Geology, vol. 19, p. 855-858.

Archibald, D., James, D., and Toohey, J., 1982. The Hyland pluton Tungsten prospect, Tuna claim group, NTS 105H/16. Energy, Mines and Resources, Government of Yukon, Assessment Report 091014.

Blusson, S.L., 1968. Geology and tungsten deposits near the headwaters of Flat River, Yukon, and southwest District of MacKenzie, Canada. Geological Survey of Canada, Paper 67-22, 77 p.

Carmichael, D.M., 1978. Metamorphic bathozones and bathograds: a measure of the depth of post-metamorphic uplift and erosion on the regional scale. American Journal of Science, vol. 278, p. 769-797.

de Capitani, C. and Brown, T.H., 1987. The computation of chemical equilibrium in complex systems containing non-ideal solutions. Geochimica et Cosmochimica Acta, vol. 51, p. 2639-2652.

de Capitani, C. and Petrakakis, K., 2010. The computation of equilibrium assemblage diagrams with Theriak/Domino software. American Mineralogist, vol. 95, p. 1006-1016.

England, P.S. and Thompson, A.B., 1984. Pressure-temperature-time paths of regional metamorphism I. Heat transfer during the evolution of regions of thickened continental crust. Journal of Petrology, vol. 24, p. 894-928.

Gordey, S.P. and Anderson, R.G., 1993. Evolution of the Northern Cordilleran Miogeocline, Nahanni map area (105I), Yukon and Northwest Territories. Geological Survey of Canada, Memoir 428, 214 p.

Gordey, S.P. and Makepeace, A.J. (comp.), 2003. Yukon Digital Geology (version 2). Geological Survey of Canada Open File 1749 and Yukon Geological Survey, Open File 2003-9(D), 2 CD-ROMs.

Guidotti, C.V., 1968. Prograde muscovite pseudomorphs after staurolite in the Rangeley-Oquossoc areas, Maine. American Mineralogist, vol. 53, p. 1368-1376.

Hart, C.J.R., Goldfarb, R.J., Lewis, L.L., and Mair, J.L., 2004. The Northern Cordillera mid-Cretaceous plutonic province: ilmenite/magnetite-series granitoids and intrusion-related mineralisation. Resource Geology, vol. 54, p. 253-280.

Hart, C.J.R. and Lewis, L.L., 2006. Gold mineralization in the upper Hyland River area: A non-magmatic origin. *In:* Yukon Exploration and Geology 2005, D.S. Emond, G.D. Bradshaw, L.L. Lewis and L.H. Weston (eds.), Yukon Geological Survey, p. 109-125.

Heffernan, S., 2004. Temporal, geochemical, isotopic and metallogenic studies of mid-Cretaceous magmatism in the Tintina gold province, southeastern Yukon and southwestern Northwest Territories. Unpublished MSc thesis, University of British Columbia, Vancouver, British Columbia, Canada, 83 p.

Kretz, R., 1983. Symbols for rock-forming minerals. American Mineralogist, vol. 68, p. 277-279.

MacLeod, W.A., 1982. Cal 81-144 mining claims, Watson Lake mining district, 105H/8W. Energy, Mines and Resources, Government of Yukon, Assessment Report 090867.

Pattison, D.R.M. and Tracy, R.J., 1991. Phase equilibria and thermobarometry of metapelites. *In*: Contact metamorphism, D.M. Kerrick (ed.), Reviews in Mineralogy, vol. 26, p. 105-206.

Pattison, D.R.M. and Vogl, J.J., 2005. Contrasting sequences of metapelitic mineral-assemblages in the aureole of the tilted Nelson batholith, British Columbia: implications for phase equilibria and pressure determination in andalusite-sillimanite-type settings. The Canadian Mineralogist, vol. 43, p. 51-88.

Rasmussen, K.L., Mortensen, J.K., and Falck, H., 2006. Geochronological and lithogeochemical studies of intrusive rocks in the Nahanni region, southwestern Northwest Territories and southeastern Yukon. *In:* Yukon Exploration and Geology 2005, D.S. Emond, G.D. Bradshaw, L.L. Lewis, and L.H. Weston (eds.), Yukon Geological Survey, p. 287-298.

Read, P.B., Woodsworth, G.J., Greenwood, H.J., Ghent, E.D., and Evenchick, C.A., 1991. Metamorphic Map of the Canadian Cordillera, Geological Survey of Canada, "A" Series Map 1714A, scale 1:2 000 000.

Roots, E.F., Green, L.H., Roddick, J.A., and Blusson, S.L., 1966. Geology, Frances Lake, Yukon Territory and District of Mackenzie. Geological Survey of Canada, Preliminary Map 6-1966, 1:253440 scale.

Spear, F.S., 1993. Metamorphic phase equilibria and pressure-temperature-time paths. Mineralogical Society of America Monograph, 799 p.

Spear, F.S. and Pyle, J. M., 2010. Theoretical modelling of monazite growth in a low-Ca metapelite. Chemical Geology, vol. 273, p. 111-119.

Strekheisen, A.L., 1973. Plutonic rocks – classification and nomenclature recommended by the IUGS's subdivision on the systematics of igneous rocks. Geotimes, vol. 18, p. 26-30.